2D Dopant Determination in Laser-Diffused Si Resistors Using Dopant-Selective Etching

Y. Liao, J.-Y. Degorce, J. Belisle, and M. Meunier[z]

Laser Processing Laboratory, Ecole Polytechnique de Montreal, Centre-ville, Montréal, Québec, Canada H3C 3A7

Two-dimensional (2D) dopant profiles, in the range of 9×10^{16} to 3.6×10^{18} atoms/cm^3, in laser-diffused silicon resistors were obtained using dopant selective etching (DSE) in combination with cross-sectional transmission electron microscopy (TEM) and focused ion beam technique. Compared with conventional DSE/TEM dopant evaluation, the properties of this technique, related to the reliability, reproducibility, and accuracy of quantification of dopant concentration from 9×10^{16} to 6×10^{19} atoms/cm^3, have been improved by considering a vector instead of a scalar etching rate, as determined by an etching model and by a novel calibration method. Those evaluated profiles were accurately compared with a numerical simulation based on heat-transfer and diffusion equations.
© 2005 The Electrochemical Society. [DOI: 10.1149/1.2128099] All rights reserved.

The National Technology Roadmap for Semiconductors[1] pointed out that requirements for the two-dimensional (2D) dopant mapping of new device generations includes a spatial accuracy of about 3 nm, and a sensitivity to doping concentrations from 10^{16} to 10^{20} cm^{-3}, as well as reproducibility of the results. In addition, for laser-diffused resistors (LDRs), which are fabricated with small laser spots (1–4 μm diam), the depth distribution of dopants, strongly determining the values of the resulted resistances, is not constant, depending on temporal and spatial temperature distribution, melting time, and dopant distribution of source and drain.[2] Many techniques available for one-dimensional (1D) dopant evaluation have not been extendable to 2D dopant characterization due to their limitations.[3] For example, secondary ion mass spectroscopy (SIMS) and spreading resistance profiling (SRP) are limited by spatial resolution. Some 2D techniques, such as scanning capacitance microscopy (SCM), could not be used for some practical microdevices, such as LDRs produced by laser fine tuning (LFT) technology[2] with small laser spot sizes, limited by the difficulties of sample preparation.

The technique of dopant-selective etching (DSE) has been used to evaluate 2D dopant profiles for several decades, even with shrinking device size. The chemical solutions were prepared by mixing oxidizing agent and HF aqueous solutions typically consisting of a mixture of HF, HNO$_3$, and CH$_3$COOH to preferentially etch exposed regions with high carrier concentrations in Si-based devices and materials. The underlying responsible mechanism is complex[4] and not completely understood, with an especially poor understanding of the etching process and the correlation between carrier concentration and the observed topography. Therefore, the accuracy and reproducibility are still very low and often different from laboratory to laboratory. A large number of etching experiments were repeated by many authors in an attempt to find suitable etch recipes with special attention paid to the preparation of the initial samples, using conventional mechanical polishing and ion milling. Samples with initial thickness of up to 1.5 μm[5] were commonly etched for 1–40 s[5-7] at selected temperatures prior to topographical measurements.

The sample topography, after the etching step, can be imaged using transmission electron microscopy (TEM), secondary electron microscopy (SEM), or atomic force microscopy (AFM). In particular, the high spatial resolution of TEM allows one to measure small changes in the thickness of material removed by the etching process to reveal many details which are not detectable by other techniques. However, there are some uncertainties in conventional DSE methodologies: (i) The etching rate was considered a constant scalar as a monotonic function of dopant concentration. In fact, the etching rate should be considered a vector with the change of direction of etch-

ing rate according to the microstructure of the exposed etched surface during the etching process. (ii) In calibration, the silicon nitride or silicon dioxide often serves as a reference for measuring the etched Si thickness.[6-8] In fact, those dielectric materials are also etched by the chemical solution even if the etching rate is lower than those of doped silicon. (iii) In calibration, the etching properties were postulated such that the silicon etching rate for both standard and testing sample depends on dopant concentration only under similar etching conditions, including sample surface preparation, temperature, concentrations of the etching solution, light illumination, agitation, etching time, sample thickness, etc. Actually, the etching behaviors could be very different even when the conditions used have only small differences.

In this paper, in order to address the requirement on device characterization in our study, as well as to improve the accuracy, reliability, and reproducibility of dopant concentration extraction, several considerations related to the mechanism of the DSE/TEM technique are addressed: (i) The chemical etching behavior has isotropic properties and the etching rate is considered as a vector; therefore, the direction of the absolute etching rate is assumed to be perpendicular to the local exposed surface of doped and undoped silicon material. (ii) The etching time and TEM sample thickness are optimized in order to obtain highly accurate doping evaluations by doping-dependent etching. The initial TEM sample thickness, prior to DSE processing, was directly measured at the end of the FIB-TEM sample preparation. (iii) The successive maxima and minima in intensity, the bright and dark fringes are plotted; and finally, this technique is applied to evaluate dopant concentrations of LDRs in comparison with numerical simulations.

Experimental

In this section, all experimental details, including a detailed modeling and calibration, are given. The technique developed will be used to profile the dopant distribution in LDRs and could also be used for any actual complementary metal oxide semiconductor (CMOS) microdevices.

Experimental details.— The calibrating standards were made using an n-type Si(100) wafer starting with a resistivity of 10 Ω cm, implanted with boron (B) at 20 keV at a dose of 5.0×10^{14} atoms/cm^2, followed by rapid thermal annealing (RTA) at 900°C for 30 s. Those specific fabrication parameters were similar to the processing conditions for fabricating heavily doped regions of CMOS devices, the nominal source and drain regions, used in producing the LDRs.

TEM samples, with a wide range of uniform thicknesses, were prepared by a Hitachi FB-2000A FIB instrument using Ga ion-beam milling. There are several principle advantages in this sample preparation, in combination with DSE technique for dopant calibration, and thus distribution quantification. First of all, as opposed to con-

[z] E-mail: michel.meunier@polymtl.ca

ventional sample preparation, the initial foil thicknesses can be directly measured during FIB-sample preparation before DSE and TEM imaging. As we had shown, this step is important because the chemical solution could attack all of the materials in integrated circuit (IC) devices, including silicon nitride and silicon oxide, at different etching rates, which will affect the reliability and reproducibility of dopant analyses. Second, starting thin films with accurately equal thicknesses and high surface quality can be prepared and reproduced. In highly accurate and highly reproducible dopant evaluation, a TEM sample film with equal starting thickness, which should be 600 nm or less as shown below, is important to avoid initial fringes which might be created by Ar+ milling caused in the conventional sample preparation process. The thickness fringes raised from initial TEM samples, if present, interfere with the interpretation of the thickness fringes created by selective chemical etching in regions being analyzed. Third, wedge-shaped samples with exactly equal wedge angles can be prepared, which is used for dopant calibration. Using the lift-out technique[9] of FIB-TEM sample preparation, two wedged samples were mounted in the same molybdenum (Mo) TEM sample grid prior to the final milling steps. This calibration method has higher accuracy than that used in conventional dopant calibration by AFM[6] due to tip shape effects in the latter. Finally, FIB can be used to prepare a specific site in a microdevice such as laser locally diffused areas with high precision.

The selectively etched samples were analyzed using a Philips CM30 TEM system operating at an accelerating voltage of 300 kV. Due to the marked dependence of the effective extinction distance (ξ_{eff}) on the transmission diffraction condition, the multibeam excited zone axis condition is used to obtain high spatial resolution. In this study, all TEM images were taken on the $\langle 011 \rangle$ zone axis, and the diffracting condition for such thickness fringes are typically seven beams selected by the objective aperture. Therefore, the number of equal thickness fringes and hence, the capacity to measure small variations of thickness, may be maximized by the reduction in ξ_{eff} resulting from on-axis imaging. As a consequence of the 1D SIMS boron profile taken from the standard wafer, the 2D dopant concentration profiles of LDRs were then extrapolated by following the equal thickness fringes far from the laser-diffused areas.

Etchant chemistry and surface quality.— HNO$_3$ drives the oxidization of silicon to form SiO$_2$, while HF attacks oxide with a lower activation energy, so that the selectivity is mainly controlled by the HNO$_3$ solution. A wide range of mixture ratios of hydrofluoric acid (HF), nitric acid (HNO$_3$), and acetic acid (CH$_3$COOH) (collectively, HNA) were tested before the final analysis. When the concentration of CH$_3$COOH in the solution is too high or when the chemical etching process occurs under dim illumination, the etching rate becomes low and the dynamic range of dopant-reflecting selectivity is reduced; furthermore, Si was mainly amorphized with the probable introduction of porosity under the stain-etching process.[10] Therefore, TEM images taken from those etched samples are not ideal for dopant concentration evaluation. The experimental results reported here are obtained from a mixture of HF (49%), HNO$_3$ (70%), and CH$_3$COOH (80%), with ratio of 1:3:8, under standard clean room conditions involving ambient illumination and a temperature of 21 ± 1°C. The reproducibility of the DSE process is ensured by maintaining constant ambient conditions.

The etching behavior of doped silicon may also be significantly affected by the initial surface conditions, including surface roughness and damage. The etching selectivity depends only on the electrically activated boron,[11] and it is lost when silicon is amorphous. In order to avoid Ga deposition and Si electrical damage on the FIB-prepared TEM sample surface, cross-sectional observation should be avoided and the milling beam should be aligned[12] and parallel to the surface being milled. Moreover, one low-current beam (0.346 nA) is used at the final milling step. Before final dopant selective analyses, AFM indicated that the root-mean-square (rms) surface roughness was less than 0.7 nm over a scan area of 1 × 1 μm for each sample, better than that of a sample surface

prepared by conventional mechanical polishing with 0.05 μm colloidal silica. The Ga contamination on the surface that could affect the DSE process is minimal, because no Ga signal was detected by energy-dispersive X-ray spectroscopy (EDX), having a sensitivity of ~0.1 atom %, and no Ga precipitates were formed on the sample surface, as verified by TEM observation.

Determination of etching time and TEM sample thickness.— In this study, the model by considering the etching rate as a scalar is called the scalar model and the model by considering it as a vector is called vector model. Based on the simulation study of the chemical etching behavior related to the vector model, one knows that the etching time and TEM sample thickness are two important factors affecting the reliability of nonuniform dopant extraction.

The thinned thickness due to selective etching was measured by wedge-sample preparation and TEM imaging. Concerning TEM sample preparation, a notched Mo TEM sample grid, shown in Fig. 1a, is first milled to obtain one concave hole (two holes for calibration), following which, the TEM sample, obtained by lift-off from the IC, is mounted in this hole, using W deposition by FIB. Then the TEM sample is thinned to various shapes, as shown in Fig. 1b and d, for the purpose of obtaining a calibration of heavily doped regions and dopant evaluation of LDRs, respectively. Both figures are described later in this paper. In order to measure the etched thicknesses related to the etching rates, TEM samples, as shown in Fig. 1b, were wedge-shaped with the angle β = 10° after final milling. Figure 1c shows one example (taken from the heavily doped regions of non-irradiated device as indicated in the frame part of the inset schematics at the right top corner) of the etched shape after the selective etching process. As expected, the hole in the doped region also shows a wedge shape. At the thin side of the samples, both the heavily doped region and the low-doped regions are completely etched by the chemical solution; however, at the thick side, only the heavily doped regions were completely etched away. Those different behaviors reflect the variation of the dopant concentration as a function of depth, considering that for a given depth the dopant concentration remains constant. Along the hole edge in Fig. 1c (indicated by the dots), the measurement of *l*, which is the distance between the dots and edge of the initial sample, permits calculation of the etched thicknesses *d* by using the equation

$$d = 2l \cdot \tan(\beta/2) \qquad [1]$$

Here, *d* is the total etched thickness from the two sides, and *l* is the vertical distance from the initial edge of the wedge sample. This calculation takes into account the 3D attack of the etching solution on the TEM samples.

Figure 2a shows the dopant profile from the boron concentration peak to the silicon bulk of the standard wafer, described in the section on experimental details, above, obtained by SIMS measurement. We assume the etching rate is a vector, perpendicular to the local etching surface, and the vector direction changes in 2D plan (*f* and *g* coordinates). At the beginning of the etching process, the rate vector is normal to the FIB-prepared flat sample surface, expressed as $v_\perp$; however, the etching direction changes depending on the etched surface shape related to the etching history of each etching site and its adjacent sites in *g-f* plan. Therefore, the etching rate vector can be transformed into two components, $v_\perp$, perpendicular to, and $v_{//}$, parallel to, the sample surface, which may be expressed as follows

$$v_{//} = \frac{\partial g}{\partial t} = V(c,t,\mu) \sin \alpha \qquad [2]$$

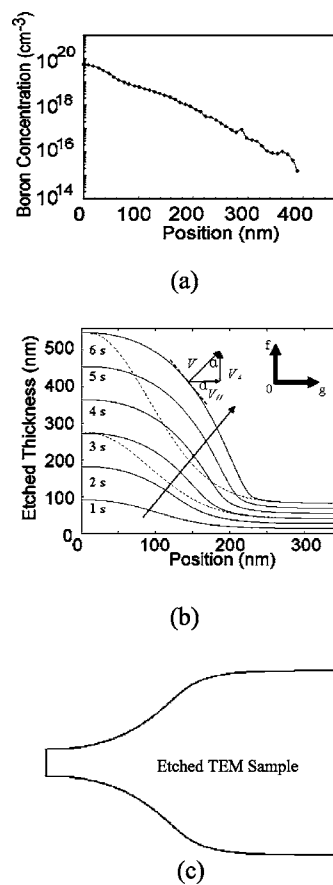$$v_\perp = \frac{\partial f}{\partial t} = V(c,t,\mu) \cos \alpha \qquad [3]$$

where α is the angle between the tangent line, corresponding to the etching interface between the silicon and the chemical solution, of the local etching site and the initial surface of the cross-sectional sample, as shown in Fig. 2b. $V(c,t,\mu)$ is the absolute etching rate
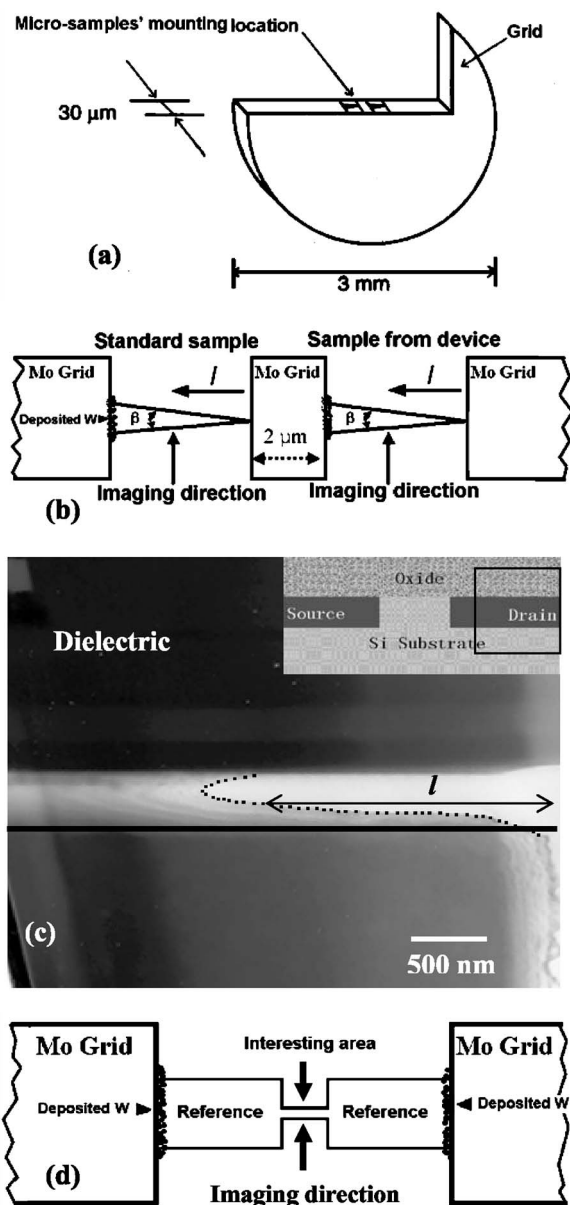
Figure 1. Schematic illustration of etched thickness measurement method due to chemical-selective etching. (a) Side view of notched TEM sample grid for microsampling. (b) Top view of TEM samples mounted in the grid after wedge-shaped milling process. (c) Cross-sectional TEM image of wedge-shaped sample after selective etching for evaluating thickness as a function of depth. (d) Top view of TEM sample used for dopant evaluation of microdevices.

Figure 2. Simulation of DSE behavior performed on a cross-sectional standard sample. (a) Partial SIMS boron concentration profile of the standard sample from the distribution peak toward the bulk silicon. (b) The solid curves along the arrow indicate the etched thickness after 1, 2, 3, 4, 5, and 6 s chemical etching simulated by the vector model using two differential equations, and dash-dot curves along the arrow indicate the etched thickness after 3 and 6 s chemical etching simulated by the scalar model. (c) Schematics of TEM sample after DSE-etched from both sides.

at position (g) reflecting the dopant concentration (c), the etching time (t), and other parameters (μ) such as the chemical solution, the temperature, etc.[5-7,13] The calculations of this simulation are based on the absolute etching rate, which is extracted using a vector model and Eq. 1, from the etched structure and dopant profile in Fig. 2a, after 3 s of chemical etching.
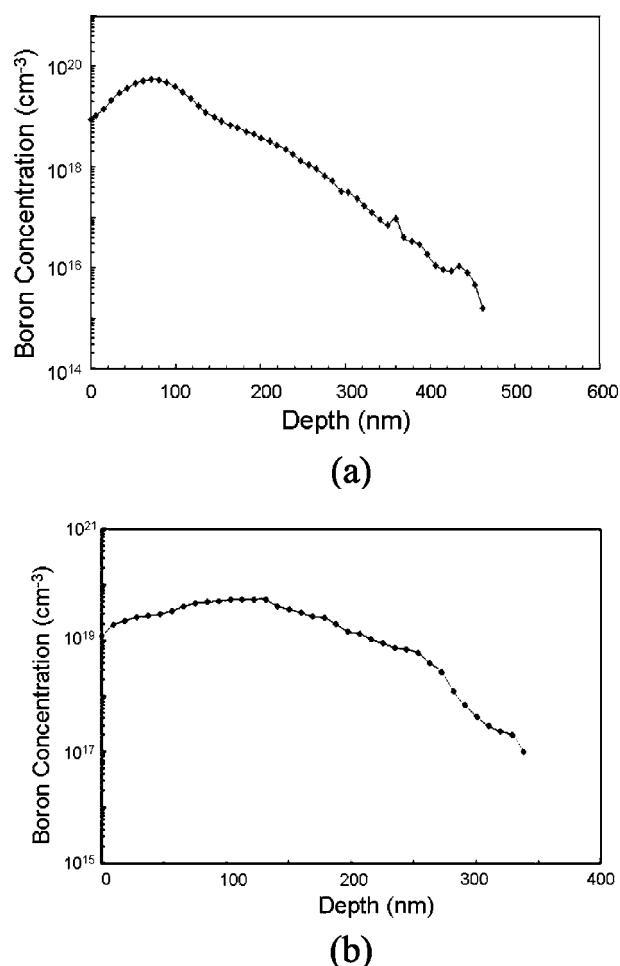
By solving the two differential equations above, the time-dependent etching thickness at each position can be obtained. We assume that the absolute etching rate under certain etching conditions is independent of etching time. Therefore, the absolute etching rate is only a function of position, corresponding to the dopant profile under certain etching conditions. In order to clearly illustrate the simulation data of the etching behavior, as shown in Fig. 2a, only the dopant profile from the concentration peak toward the bulk sili-

con, extracted from Fig. 3a, is used. The positions in Fig. 2a and b represent the depth of the local point from the dopant distribution peak. The simulated curves, using this dopant profile, are shown in Fig. 2b.

The solid lines in the arrow direction reflect the etched silicon thickness based on a vector model, containing $v_\perp$ and $v_{//}$ factors, determined by Eq. 2 and 3, respectively, after 1–6 s of chemical etching. The two dot-dash curves along the arrow direction indicate the etching thickness after 3 and 6 s chemical etching, simulated using the scalar model with conventional scalar etching rate $V(c,\mu)$. As shown in Fig. 2b, the difference of the computed etched thickness obtained from the two models becomes greater with increasing etching time. The most significant difference is in the middle region, between the two locations with the highest and lowest dopant concentrations. Furthermore, the sensitivity of the dopant selective etching technique for electrically activated boron atoms, indicated by the deepest visible thickness fringe close to the undoped bulk Si side, is 9×10^{16} atoms/cm^3 in concentration, located at a depth of 254 nm. However, the last possible thickness fringe after 6 s or longer etching time, deduced from the simulation, moves to the right side, leading to a bigger etched hole. Another issue, which should be considered, is that the etching time should be long enough to have final thickness variations, among areas with different doping levels, greater than the extinction distance for observing the fringes. The model presented in this paper is similar to the one recently published by other researchers.[14] In practice, for the dopant characterization of
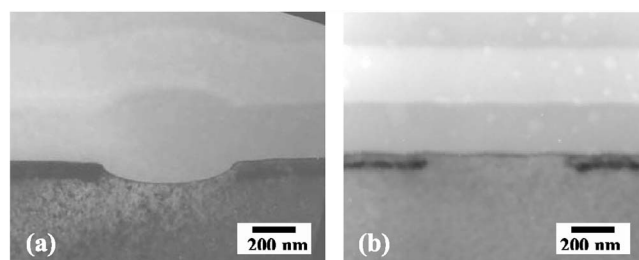
Figure 3. (a) SIMS profile shows the 1D boron distribution in standard sample. (b) Calibrated 1D boron profile in the heavily doped regions of nonirradiated devices.
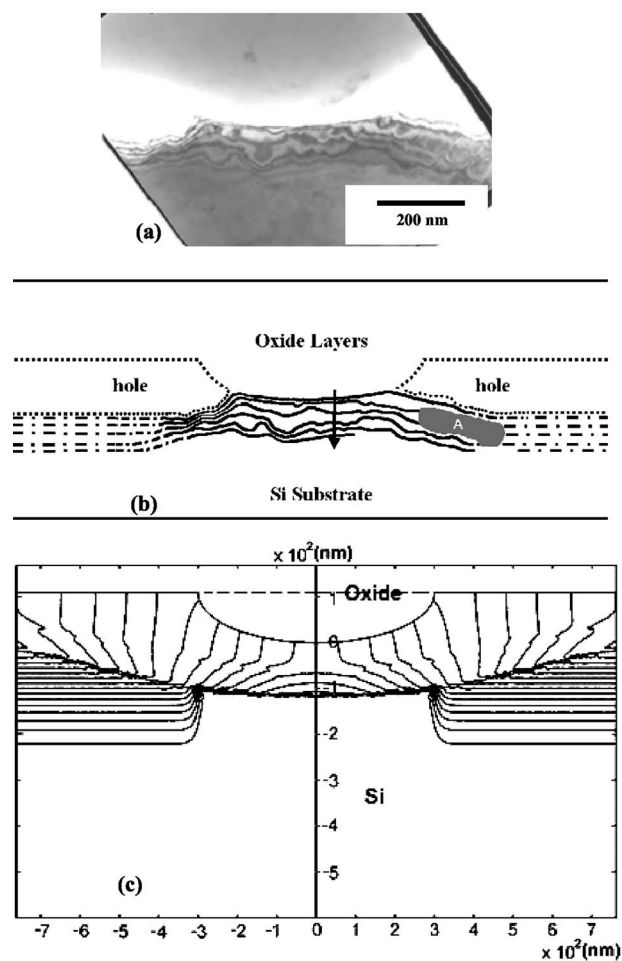

Figure 4. Two different types of microdevices before LFT process: (a) field-effect device and (b) flat device.

As schematically shown in Fig. 1b, two TEM samples, one taken from the standard wafer and one from the source/drain regions in a non-laser-irradiated device, with a small distance of about 2 μm between both samples were prepared and mounted on the same notched Mo grid, shown in Fig. 1a, using tungsten (W) deposition by FIB. The two TEM samples were then wedge-shaped, with the same angle ($\beta = 10°$) after final milling. These TEM samples were used to calculate the etched thickness, by using Eq. 1, for dopant calibration. In addition, according to the principle of our vector simulation analysis, the etching behavior of any local point is affected by the adjacent points. Therefore, in order to have a high accurate calibration, the two TEM samples should have similar dopant concentration gradients. In this way, the related etched thicknesses are accurately obtained under the same chemical etching conditions, including HNA components, temperature, illumination, and 3 s of etching time, by following the method described above. The dopant profile, from low dopant concentrations to high dopant concentrations in the non-laser-irradiated source and drain regions of the LDRs (which is discussed in the next section), is calibrated by the 1D SIMS dopant profile of the standard sample shown in Fig. 3a and quantified as shown in Fig. 3b. The reason that the profile contains a smooth peak is possibly that boron atoms, in the high-dopant-concentration region, are not fully activated and/or the etching rate is saturated. From the dopant profiles it can be deduced that the ranges of the dopant concentrations between the sample taken from our device and the sample taken from the standard wafer are almost the same; however, the doped depths between them are different. Based on our experiments, the calibrated data obtained by our novel method are more reproducible, reliable, and accurate than those obtained by other techniques such as SCM, limited by sample structure, and AFM in combination with DSE, limited by the tip shape. Our calibration measurements have been repeated four times and all the profiles are similar, with an error of less than 5%.
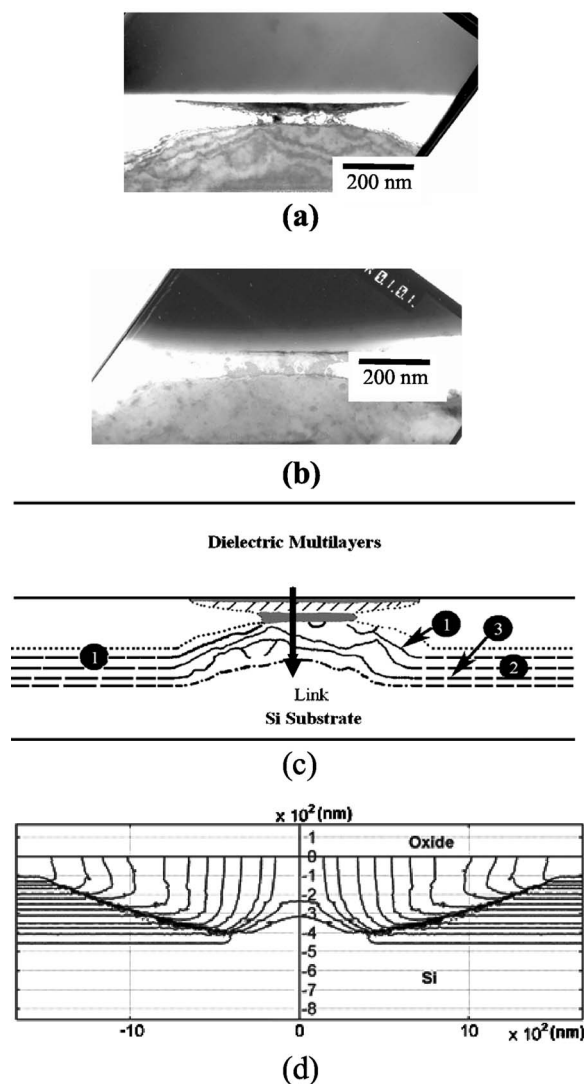
Dopant Profiling of LDRs

Figure 4 shows the cross sections of two different types of gateless transistors with a nominal source to drain distance of 0.6 μm. The rounded shape of the oxide layer in Fig. 4a is caused by the field oxidation process and was used to mask the implants (boron atoms) due to the absence of the gate between the highly doped regions. Figure 4b shows one flat device with two heavily doped regions. The doping atoms diffuse from the highly p-type doped regions to the lightly n-type doped gap region when a laser beam is focused on the center of the gap region and the edges of the adjacent heavily p-type doped regions connecting to the gap;[2] thus, a resistive link with a medium dopant concentration is formed. Field-effect and flat LDRs, with resistances of 500 and 230 Ω, respectively, are produced with 100 laser pulses, 3.0 W of power, and 80 ns of a pulse width, and are analyzed in this study.

Before dopant analysis, the TEM samples taken from LDRs were observed using TEM and had not significant structural differences from the non-laser-irradiated devices shown in Fig. 4. During DSE, the Si material close to the dielectric/Si interface in the heavily doped source and drain regions, adjacent to the resistors, would be

industrial shallow junction and LDRs, the optimized etching time is 3 s, which gives a good compromise between the reliability of the dopant extraction and the fringe formation. It was verified, by vector simulation, that the inaccuracy of the extracted dopant profile due to the etched hole is less than 1% when the etching time is 3 s. The etching time is controlled by using a tenth-second timer with an error of less than 5%, which is reasonable to ensure a uniform and reproducible wet etching process.

A further consideration is the TEM sample thickness. As is well-known, the dopant concentration extraction technique is based on the etched TEM shape and thickness fringes observed under electron diffraction. Because of the decrease in intensity, due to factors such as inelastic scattering,[15] with an increase in sample thickness, the TEM sample cannot be too thick. The acceptable range of the initial TEM sample thickness for dopant concentration analysis for the LDRs is around 600 nm. For an etching time of 3 s and an initial TEM sample thickness of 600 nm, the sensitivity of boron evaluation based on this technique is 9×10^{16} atoms/cm^3, by considering that the TEM samples are etched from both sides as indicated in Fig. 2c, which can satisfy the LDRs, as well as other microdevices.

Calibration.— In order to determine the quantitative dopant concentration in the resistive link formed by laser technology, it is necessary to calibrate the dopant concentration in the nominal source/drain regions. For highly accurate calibration, the samples must have similar structures and similar dopant concentration gradients. The 1D dopant profile of the standard sample as shown in Fig. 3a was obtained using SIMS.

(a)

200 nm

(b)

Figure 5. (a) TEM image revealing thickness fringes as a result of dopant-level-dependent etching for 3 s. (b) Skeletonized micrograph showing the extracted dopant isoconcentration contour of the LDR. (c) Simulated 2D dopant profile.

Figure 6. (a) TEM multibeam image taken from one flat LDR after DSE, (b) one-beam TEM image showing the left etch-amorphized material in the upper part of the resistive link, (c) plotted dopant profile corresponding to the TEM images, and (d) simulated 2D dopant distribution.

completely etched away, losing the reference for measuring the etched depth. To overcome this problem, two very thick areas in source and drain regions, as shown in Fig. 1d, were also prepared by FIB; because these thick areas were essentially not affected by the 3 s of chemical etching process, they can be used as references for measuring the depth of all the fringes. Following 3 s chemical etching, Fig. 5a shows the multibeam TEM image of one LDR. Corresponding to the structure of Fig. 4a, the microresistor formed is located underneath the dielectric and between the two heavily doped regions. First, the fact that we observed a regular distribution of fringes precludes the possible effect of gallium, which should give a uniform distribution if its incorporation into the sample was high enough due to ion-beam milling. These fringes are clearly related to the dopants that have diffused from the two heavily doped regions. In the resistance region, there are six dark fringes observed after the DSE process. The last equal thickness fringe indicates that the laser-molten depth is 113 nm underneath the interface between the dielectric and the diffused resistor. In this device, the effective resistance length, which is considered to be the region with a dopant concentration lower than that along the dotted curves, between the hole and silicon material left, with a boron concentration value of 5.9×10^{18} atoms/cm^3, is 417 nm. By following the equal thickness fringes in the heavily doped regions without laser irradiation, far from the laser-molten areas and indicated as dash-dot curves in Fig. 5b, isoconcentration profiles, corresponding to the equal thickness profiles in the diffused resistance link, are obtained. Isoconcen-

tration curves, delineated as solid lines, were plotted from the dark fringes of the original TEM micrograph shown in Fig. 5a. Moreover, the dopant concentrations corresponding to from the first to sixth solid curves marked by the direction of the arrow in Fig. 5b, are 3.6, 1.8, 0.65, 0.36, 0.36, and 0.24×10^{18} atoms/cm^3, located at depths of 0, 8, 38, 83, 101, and 113 nm, respectively. The reason that curve 4 has the same dopant level as curve 5 is that both of them are extended from the same dopant level curve in the heavily doped region, which could be seen on the left side of the resistive link. The gray area marked A has an almost uniform dopant concentration, with a value of 1.8×10^{18} atoms/cm^3, determined by following the dark fringe 2. Figure 5c corresponds to a simulation result and will be introduced in the following section.

Figure 6a shows one multibeam TEM image after selective etching performed on a flat LDR with the initial structure shown in Fig. 4b. The dash-dot curve in Fig. 6c obtained from the last fringe, which is a white equal thickness fringe in Fig. 6a, indicates that the maximum molten depth along the arrow is 270 nm. The dopant concentration along the boundary between the etched hole and the left silicon materials is 8.9×10^{18} atoms/cm^3. Along the arrow there are four areas: two gray areas, one shaded area, and one fringed area. Figure 6b was taken from one beam imaging condition;
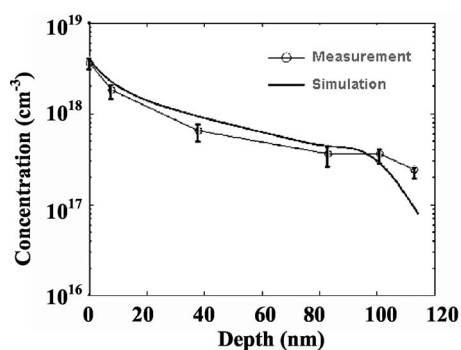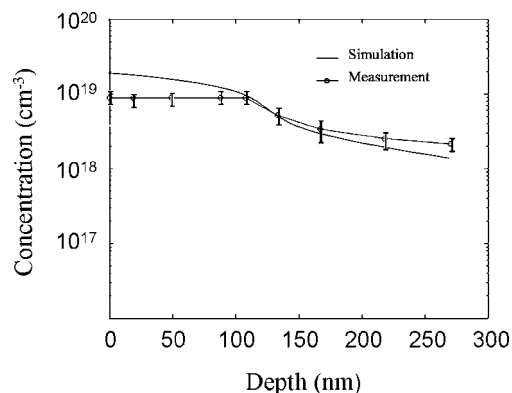
Figure 7. 1D experimental dopant profile along the arrow in Fig. 5b and simulated depth profile along the melting center in Fig. 5c.

Figure 8. Quantified dopant depth profiles (1D) along the arrow and along the melting center in Fig. 6c and Fig. 6d, respectively.

there is no diffraction contrast and, thus, the contrast reflects mainly the material thickness. This image shows that the material thickness in the three upper areas (two gray areas and one shaded area) is almost uniform, indicating that the net electrically activated dopant concentrations in these three areas are nearly uniform. The two gray areas in Fig. 6a do not present diffraction contrast and, in the shaded area, dark contrast is visible under multibeam diffraction conditions. It is believed that the materials in the two gray areas are thin and amorphized after chemical etching.[16] The upper gray area was etched at a high rate due to the high concentration of vacancies formed under laser irradiation. The lower gray area contained electrically activated boron atoms with a little higher concentration than the fringed area. The shaded area contained thicker silicon material than the lower gray area, revealed by diffraction contrast from the local crystalline film, probably because acceptors were partially compensated by oxygen-related donors[17] formed due to oxygen diffusion from dielectric layer during laser irradiation. Because the thicknesses of the two gray areas and the shaded area were almost completely etched, the dopant concentration in these three areas could be considered the same as that of the boundary between the hole and the left silicon material of the fringe area, which is 8.9×10^{18} atoms/cm^3. The dopant concentrations of the solid curves 1, 2, and 3 in Fig. 6c are 7×10^{18}, 3.4×10^{18}, and 2.6×10^{18} atoms/cm^3, respectively. The dopant concentration of the dot-dash curve, plotted according to the white fringe in Fig. 6a, is 2.2×10^{18} atoms/cm^3. Figure 6d corresponds to a simulation result and will be introduced in the following section.

Discussion

Previously, our research group[18] studied laser-induced melting and solved the heat-transfer equation to obtain the 3D out-of-equilibrium transient temperature field $[T(r,t)]$. It has been shown that the actions of heat-transfer from laser to materials as well as from molten pool to solid Si substrate can be described accurately with the modeling. Knowing $T(r,t)$, one can use Fick's law $\partial C/\partial t = -D \nabla C$ to obtain the boron profile by considering that the dopants diffuse in the liquid with a diffusion coefficient of $\sim 3.8 \times 10^{-4}$ cm^2/s in liquid Si[19] and assume that B does not diffuse in the solid phase because the maximum diffusion coefficient in the solid at melting temperature is $\sim 4 \times 10^{-11}$ cm^2/s,[20] leading to a negligible diffusion distance $\sqrt{Dt}$ of ~ 0.03 nm with a typical melting time of 200 ns. In order to confirm the physical mechanism of the LFT process, numerical simulations were performed on dopant diffusion. Figures 5c and 6d show the simulated 2D dopant distribution obtained by considering the processing calibration given in the last section with an initial doping profile in the source/drain regions given in Fig. 3b. The spatial resolution of the developed methods for dopant calibration and 2D evaluation is 1–5 nm, depending on the local dopant concentration gradient. Using these methods, the plotted data, extracted from the dark fringes along the arrow shown in Fig. 5b, are indicated by the points shown in Fig. 7.

In addition, the plotted data, extracted from the boundaries of the areas with different contrasts (shown in Fig. 6a) and dark and bright fringes shown in Fig. 6c along the arrow positions, are shown in Fig. 8. The arrows represent the average values of dopant concentrations for all the isoconcentration curves in each device. Figures 7 and 8 also show simulated 1D profiles, plotted along the center of Fig. 5c and Fig. 6d, respectively. Obviously, isoconcentration lines in the resistive links, as shown in Fig. 5b and Fig. 6c, are not straight lines; thus, we use error bars, calculated by considering the dopant concentrations along each arrow as references, to indicate the dopant concentration variations inside the links. These dopant variations in the resistive links are first due to the diffusion of a nonuniform dopant distribution during the laser-induced melting process, as revealed by Fig. 5c and Fig. 6d, and second, due to the local nonuniformity of heat absorption and diffusion in the actual Si materials. These profiles, after considering the reasonable error, are reproducible and reliable for different fabricated resistors based on the same initial structures and laser conditions, which cannot be obtained by conventional dopant evaluation techniques. It is also verified by resistance simulation (not shown here) that the evaluated dopant profile is highly accurate. Clearly, the entire quantified experimental dopant profiles, described in Fig. 7, and the one in the deep region in Fig. 8, match the simulated dopant profiles. This indicates that the dopant concentration decreases in this melting volume when it becomes deeper. However, as indicated in the 2D dopant distributions as shown in Fig. 6c and d and the 1D profiles in Fig. 8, experimental data are different from simulated data in the near-interface region, probably due to oxygen-related donor compensation. Furthermore, from the simulations, it could be understood that under the same laser-processing conditions, the molten depth and volume in the flat LDRs are deeper and larger, respectively, than those in the field-effect LDRs, due to the light reflection difference caused by the shape difference of the laser-irradiated interface between the dielectric and Si gap. Finally, the dopant concentrations decrease with increasing depth for both LDRs, because the melting duration is shorter with increasing depth since the heat released from the molten silicon into the dielectric was much less than that into the silicon.

Conclusion

The selective etching process was modeled so that the reliability, accuracy, and reproducibility of dopant extraction by DSE have been improved. It is pointed out that when the TEM sample thickness is around 600 nm and the etching time is 3 s, the etched camber shape in the doped regions may be considered to be plane, parallel to the initial surface of the TEM sample, and thus, the etched profile can be directly measured for extracting credible dopant concentration. A novel FIB sample preparation allows one to obtain TEM samples for dopant calibration under the same chemical selective etching conditions. Finally, the developed quantification technique was used for dopant evaluation on LDRs, fabricated with small laser

spot size, and the results are in good agreement with numerical simulation obtained by solving heat-transfer problems and diffusion equations. It seems reasonable to consider the role of acceptor compensation by oxygen-related donors due to laser-induced oxygen diffusion and activation. The excellent dopant delineation shows that the improved DSE technique is a practical technique for the highly accurate quantification of 2D dopant distribution of LDRs, and we believe that it has a good potential to be effectively used for other types of microdevices.

References

1. The International Technology Roadmap for Semiconductors (http://public.itrs.net/), Semiconductor Industry Association, San Jose, CA (2004).
2. M. Meunier, Y. Gagnon, Y. Savaria, A. Lacourse, and M. Cadotte, *Appl. Surf. Sci.*, **186**, 52 (2002).
3. W. Vandervorst and H. Bender, in *Proceedings of the 19th European Solid State Device Research, ESSDERC 89*, pp. 843-860, Springer-Verlag, New York (1989).
4. D. R. Turner, *J. Electrochem. Soc.*, **107**, 810 (1960).
5. S. S. Neogi, D. Venables, Z. Ma, D. M. Maher, M. Taylor, and S. Corcoran, *J. Appl. Phys.*, **82**, 5811 (1997).
6. V. Raineri, V. Privitera, W. Vandervorst, L. Hellemans, and J. Snauwaert, *Appl. Phys. Lett.*, **64**, 354 (1994).
7. C. Spinella, V. Raineri, F. La Via, and S. U. Campisano, *J. Vac. Sci. Technol. B*, **14**, 414 (1996).
8. W. Vandervorst, T. Clarysse, J. Vanhellemont, and A. Romano-Rodriguez, *J. Vac. Sci. Technol. B*, **10**, 449 (1992).
9. M. H. F. Overwijk, F. C. van den Heuvel, and C. W. T. Bulle-Lieuwma, *J. Vac. Sci. Technol. B*, **11**, 2021 (1993).
10. S. Liu, C. Palsule, S. Yi, and S. Gangopadhyay, *Phys. Rev. B*, **49**, 10318 (1994).
11. S. Whelan, V. Privitera, M. Italia, G. Mannino, C. Bongiorno, C. Spinella, G. Fortunato, L. Mariucci, M. Stanizzi, and A. Mittiga, *J. Vac. Sci. Technol. B*, **20**, 644 (2002).
12. J. P. McCaffrey, M. W. Phaneuf, and L. D. Madsen, *Ultramicroscopy*, **87**, 97 (2001).
13. J. Liu, M. L. A. Dass, and R. Gronsky, *J. Vac. Sci. Technol. B*, **12**, 353 (1994).
14. S. Scalese, A. La Magna, M. Italia, S. Pannitteri, V. Privitera, R. Duffy, and M. J. P. Hopstakenc, *J. Electrochem. Soc.*, **152**, G277 (2005).
15. K. Nishio, T. Isshiki, and M. Shiojiri, *J. Electron Microsc.*, **49**, 607 (2000).
16. R. W. Fathauer, T. George, A. Ksendzov, and R. P. Vasquez, *Appl. Phys. Lett.*, **60**, 995 (1992).
17. Y. Mada and N. Inoue, *Appl. Phys. Lett.*, **48**, 1205 (1986).
18. J.-Y. Degorce, J.-N. Gillet, F. Magny, and M. Meunier, *J. Appl. Phys.*, **97**, 033520 (2005).
19. P. D. Mitev, M. Saito, Y. Waseda, and Y. Sato, *High Temp. Mater. Processes (N.Y., NY, U.S.)*, **19**, 307 (2000).
20. R. B. Fair, in *Impurity Doping Processes in Silicon, Materials Processing-Theory and Practices*, Vol. 2, F. F. Y. Wang, Editor, p. 338, North-Holland, Amsterdam (1981).